ICARUS **124,** 296–307 (1996)
ARTICLE NO. 0205

Deucalionis Regio, Mars: Evidence for a New Type of Immobile Weathered Soil Unit

ERZSÉBET MERÉNYI

Lunar and Planetary Laboratory, University of Arizona, Tucson, Arizona 85721
E-mail: erzsebet@lpl.arizona.edu

KENNETH S. EDGETT

Department of Geology, Arizona State University, Box 871404, Tempe, Arizona 85287-1404

AND

ROBERT B. SINGER

Lunar and Planetary Laboratory, PIRL, University of Arizona, Tucson, Arizona 85721

Received July 7, 1993; revised March 28, 1996

A small equatorial region south of Sinus Meridiani, Deucalionis Regio, has been found spectrally distinct from other regions as seen in a high spectral resolution telescopic image of Mars. Interpretations from a variety of other observations, including infrared radiometric data, historical occurrences of localized dust storms, and general circulation wind modeling, also suggest that the surface of Deucalionis Regio has properties that are different than those of nearby regions, Arabia, Acidalia, Sinus Meridiani, and Oxia, in terms of expression of color, crystalline hematite content, and perhaps pyroxene abundance and mineralogy. The thermophysical and aeolian observations indicate that the soils in Deucalionis Regio are relatively immobile, despite the likely occurrence of winds strong enough to move unconsolidated materials. We propose that the soils in this region are indurated or crusted. We predict that a Mars Observer-class thermal emission spectrometer and gamma ray spectrometer will show the presence of crust-forming minerals and elements in the soils of this region. The spatial correlation between areas that have been previously proposed to be regional exposures of crust, and areas that are spectrally similar to Deucalionis Regio, may suggest a possible genetic relationship between the composition and the physical properties. © 1996 Academic Press, Inc.

1. INTRODUCTION

The upper few centimeters of Mars, collectively termed the ''Martian surface layer,'' is considered to be largely composed of debris or ''soil,'' with limited exposures of bedrock (*e.g.*, Arvidson *et al.* 1989; Christensen and Moore 1992). In recent years, analyses of Mariner, Mars, and Viking data have matured, new observations with high spatial and/or spectral resolution have been obtained from Earth-based telescopes and Phobos 2, and more powerful computers and analysis techniques have been applied to cross-compare data sets. As a result, it is now becoming apparent that the Martian surface layer has more variations in its physical and mineralogical properties than were previously known (*e.g.*, Singer and Miller 1991; Christensen and Malin 1993; Murchie *et al.* 1993; Mustard *et al.* 1993; Geissler *et al.* 1993).

This paper highlights an example of a region that seems to have different surface layer properties than have previously been described. By bringing together a variety of observations, we have found that Deucalionis Regio is different from its surrounding regions. Deucalionis Regio is a cigar-shaped, intermediate-albedo region which runs nearly parallel to the Martian equator, just south of the low-albedo areas of Sinus Meridiani and Sinus Sabaeus (Fig. 1; Fig. 1 of Merényi *et al.* 1996; Antoniadi 1930, p. 76). Its main body extends from 330° W to 10° W across the prime meridian and between 13° S and 17° S. The western end of the ''cigar'' has a time-variable (in terms of years), narrow continuation which curves to the northwest at a nearly right-angle toward Oxia Palus to form the southern and western borders of Sinus Meridiani (Antoniadi 1930, p. 77; Baum *et al.* 1970; Kieffer *et al.* 1981).

Our attention was originally drawn to Deucalionis Regio as a result of mixing model analyses of a 0.44 μm to 1.04 μm spectral image of Mars obtained by telescope during the 1988 opposition (Singer *et al.* 1990), in which it was found that the region could not be modeled as a simple

0019-1035/96 $18.00

linear mixture of materials observed in the large, ''typical'' albedo units such as Arabia and Sinus Meridiani (Merényi *et al.* 1992, 1996). Prior to this observation, the surface soil properties of Deucalionis Regio received little attention in the spacecraft-era Mars literature, perhaps owing to its nondescript appearance in orbital imaging. Deucalionis Regio (Fig. 1) is striking only in its relative blandness: it is a heavily cratered region (Murray *et al.* 1971) with few color and albedo variations (Fig. 1).

In this paper, we present summaries of visible, near-infrared, thermal infrared observations and derived maps for the region which includes Deucalionis Regio. We also discuss the historical occurrence of local dust storms and surface wind shear derived from general circulation models for the vicinity of Deucalionis Regio. We conclude that the regional surface layer is (*a*) different in terms of surface exposure of crystalline hematite- and possibly pyroxene-bearing materials, and (*b*) is probably composed of an indurated or crusted soil which inhibits aeolian erosion. The lack of aeolian disturbance or deflation is likewise controlled by the absence of loose sand which would otherwise saltate, sort, and erode the soil. These conclusions allow us to propose hypotheses which can be tested with anticipated future spacecraft observations. We also suggest that the spatial correlation between areas proposed to be regional exposures of crust and areas that are spectrally similar to Deucalionis Regio may indicate a possible genetic relationship between the composition and the physical properties.

2. VISIBLE/NEAR-INFRARED SPECTRAL PROPERTIES

2.1. Results From Spectral Analyses

The apparent uniqueness of Deucalionis Regio was brought to attention by analyses of a telescopic spectral image acquired during the 1988 Mars opposition (07:21–08:08 UT 26 September) by Singer *et al.* 1990. The image, its calibration and other pertinent information are described in the companion paper by Merényi *et al.* (1996). Linear mixture model analysis of our 1988 spectral image of Mars, also discussed in detail by Merényi *et al.* (1996), shows that this scene is well modeled by endmember spectra from Western Arabia, South Acidalia and Sinus Meridiani. This model, however, yields large errors in the Deucalionis Regio area and, to a lesser extent, in Chryse/Xanthe, Oxia, and Noachis. Selection of an additional endmember spectrum from Deucalionis (15° S, 345° W) resulted in a model fit within 5% residual error for all pixels with 1.1% mean absolute residual and 1.5% standard deviation across pixels and with endmember fractions between 0 and 1 within the noise limit. As shown in Fig. 2a, Deucalionis Regio is distinguished from the other regions, and the same ''Deucalionis material'' is also found in Noachis, and in somewhat smaller concentrations in Oxia and Chryse. The part of Noachis that maps as spectrally similar to Deucalionis extends roughly over the larger light green segment on Fig. 2b, between 20°W–340°W and 30°S–50°S. For clarity, we will refer to this region as ''western Noachis'' in this paper. Quantitative examination of the Deucalionis endmember shows over 50% contribution in Oxia, Chryse, and western Noachis. Western Noachis in particular seems to be a contiguous area of uniformly high Deucalionis fractions.

An independent supervised classification with an artificial neural network for the same image separated eight spectrally distinct units with geological interpretation. All pertaining details of this classification are given in Merényi *et al.* (1996). In Fig. 2b, the color-coded units show the classes which, we wish to emphasize, map spectral types and not strictly geographical units. For example, the ''Chryse class'' maps the occurrence of spectra similar to the training spectra for this class, taken from the middle of the Chryse basin (40° W, 17° N). The main spectral types that are relevant to this study are shown in Fig. 3. These are averages of the typically 5–10 training spectra for each of the corresponding classes from Fig. 2b. The averages of the spectra within the corresponding classes are virtually identical to these (see Fig. 9 in Merényi *et al.* 1996), which indicates high accuracy of the pattern recognition. Comparison with Fig. 2a shows that the spectral types used in the linear mixture model (Arabia, Sinus Meridiani, Acidalia, and Deucalionis Regio) are mapped similarly by the neural network classification, with further subdivisions for the Sinus Meridiani and Deucalionis Regio classes, and additional classes (e.g., condensates). The two subclasses of Deucalionis, DR and DR2 (green and dark green on the map), are conspicuously separated by latitude, with DR2 dominating near the equator, north and west of Sinus Meridiani. These two classes are both very tight (i.e., the standard deviation is small for each class) even though DR extends over a large area. They are too similar for the linear mixing model to separate, still, there is a consistent and real spectral difference between them detected by the non-linear pattern recognition method.

2.2. Viking Image Color

Arvidson *et al.* (1989) and Presley and Arvidson (1988) described the Mars surface layer in regions to the northwest of Deucalionis Regio, based on Viking 3-color images. They identified three basic color units: Bright Red, Dark Red (or Brown), and Dark Gray. It was generally interpreted that the Bright Red surfaces, as found covering most of Arabia, are characterized by optically thick, unconsolidated dust storm fallout or other chemically weathered soil, while Dark Gray units probably contain exposures of relatively unweathered mafic material. Exposure of rocks, as modeled from thermal IR data, is lowest in regions of

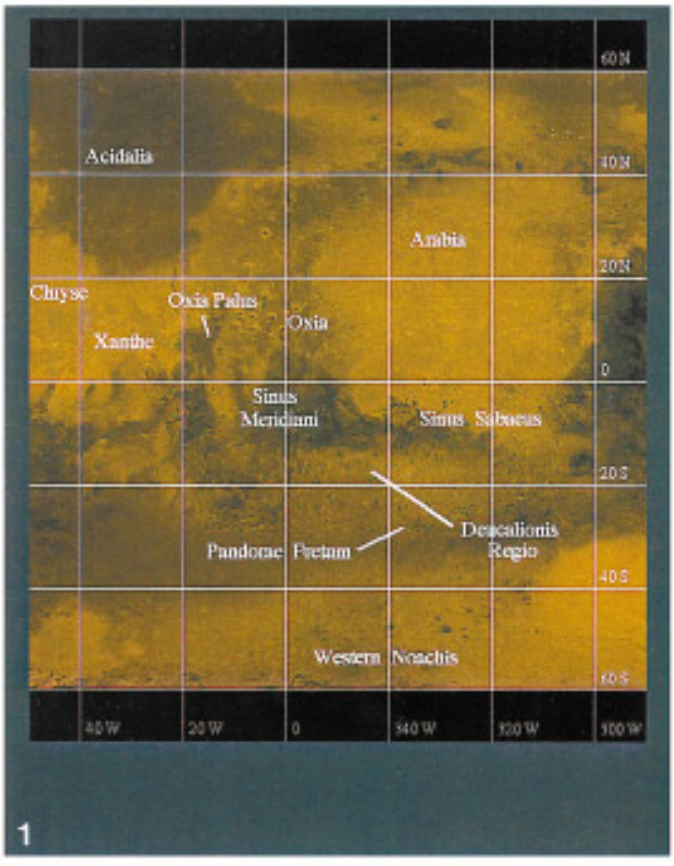
Acidalia
Arabia
Chryse
Oxia Palus
Oxia
Xanthe
Sinus Meridiani
Sinus Sabaeus
Pandorae Fretum
Deucalionis Regio
Western Noachis
60 N
40 N
20 N
0
20 S
40 S
60 S
40 W
20 W
0
340 W
320 W
300 W
1

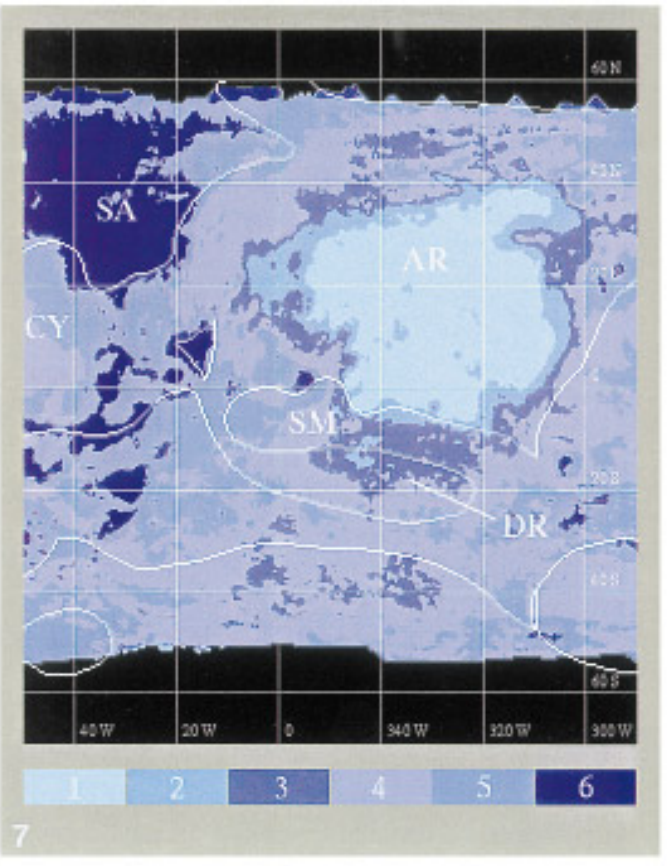
SA
AR
CY
SM
DR
1
2
3
4
5
6
7

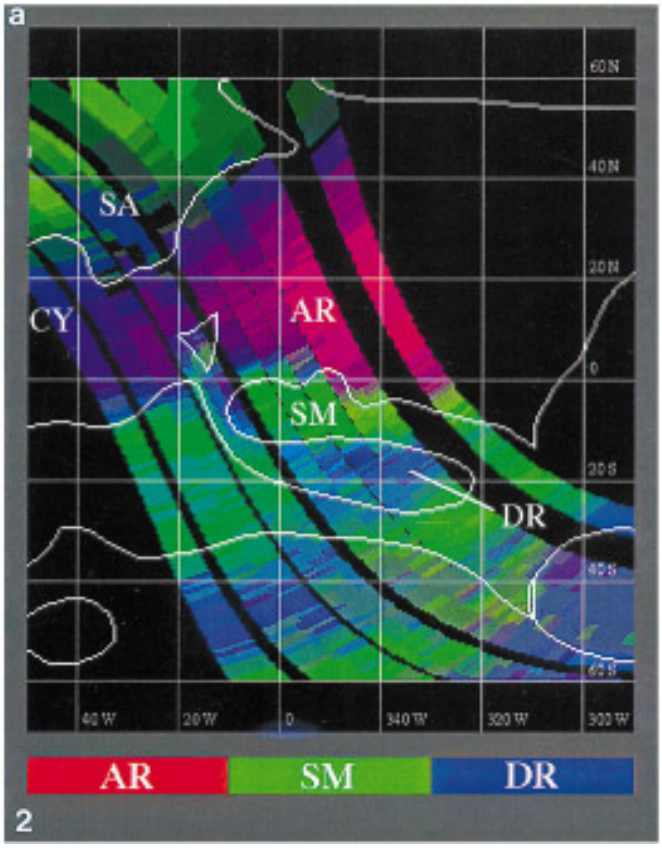
a
SA
CY
AR
SM
DR
AR
SM
DR
2

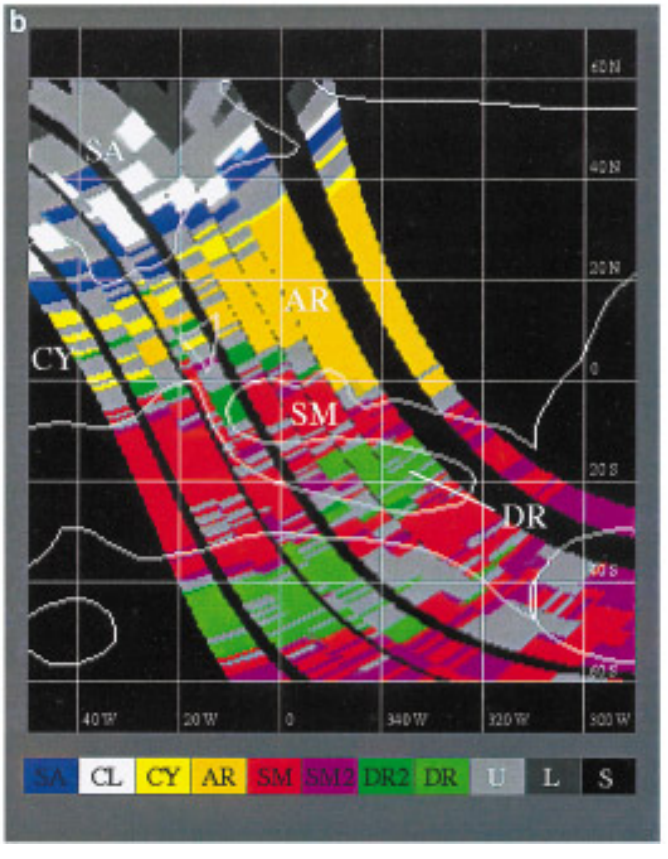
b
SA
AR
CY
SM
DR
SA
CL
CY
AR
SM
SM2
DR2
DR
U
L
S

considerable dust (Arabia) or sand cover (Sinus Meridiani), and greatest in Dark Gray regions of modest sand cover (Acidalia) (Christensen 1986a). The Dark Red unit, observed in Lunae Planum, Chryse, and Oxia, was interpreted to be a mixture of Dark Gray and Bright Red materials and/or regional exposures of Bright Red materials that are now crusted and roughened by aeolian erosion (Singer *et al.* 1984; Presley and Arvidson 1988; Arvidson *et al.* 1989). Photometric properties interpreted from Viking color images support this interpretation of physical roughness. At very low phase angles (1°) Dark Red exposures have red/violet ratios (R/V) and albedo which are fairly similar. Dark Red also falls on a color mixing line between Bright Red and Dark Gray. At higher phase angles, however, the color and albedo differences become greater, consistent with greater sub-pixel roughness in Dark Red leading to a higher percentage of unresolved shadows (Arvidson *et al.* 1989).

In a qualitative sense, Deucalionis Regio does not seem to fit the three-unit color classification of Arvidson *et al.* (1989). A Viking color image (Fig. 1) compiled by McEwen *et al.* (1993) shows that this region is not as bright as Arabia, and is less dark than Oxia. Antoniadi (1930) also noted that this region has a distinctly different color through the telescope from the surrounding areas, and McCord *et al.* (1982a) found color differences in their analysis of Viking 2 approach mosaic.

2.3. Mineralogic Implications of the Spectra

The ratio of Deucalionis Regio spectra to spectra of other regions provides some information about mineralogical differences. The spectral shapes of the main units can be seen in Fig. 3. Because the spectra were normalized for brightness (see Merényi *et al.* 1996), we can strictly compare their spectral properties. Interpretation is based on broad spectral features and continuum shapes, while small, high-frequency variations (due to noise and residual atmospheric and stellar lines) are disregarded. The subtle but real differences among these spectra, on the order of a few percents, are enhanced in ratios. Ratioing class averages rather than individual selected spectra can suppress noise enough to reveal the subtle features that may not be seen clearly from ratios of single spectra.

Figure 4 shows that Deucalionis Regio relates to the other units in varied ways. One obvious observation is that the depth of the Fe^{3+} absorption band near 0.53 μm varies according to region (as noted by Singer and Miller 1991), indicating that crystalline hematite concentration in Deucalionis Regio is different from other regions in this study. In the ratio spectra, the sharper the bend near 0.53 μm, the larger the relative difference in crystalline hematite content between the two regions. Deucalionis appears to have the most crystalline hematite among the regions studied here (Merényi *et al.* 1996). Quantitative evaluation of the hematite abundances is difficult, because of the strong dependence on particle size and mixing geometry (Morris and Lauer 1990). However, it has been estimated by Singer and Miller (1991) that the differences observed in this data set are likely caused by hematite abundance variations of a few weight percents.

The ratio spectra also show some differences in behavior between about 0.8 and 1.0 μm, which can indicate relative differences in pyroxene abundance and/or composition (e.g., Burns 1970; Adams 1975). Detailed interpretation of

FIG. 1. Mars color from Viking images. Deucalionis Regio has an intermediate color and albedo relative to Arabia, Sinus Meridiani, and other bright and dark regions. Deucalionis Regio is distinct in its relative lack of dark deposits on crater floors or in other topographic traps. Such dark incrater deposits are common in most other cratered regions, including a few examples in Arabia (see Edgett and Christensen, 1994). Note that the color is not as it would appear to the human eye from Mars orbit, as the green band used in this image is synthetic and the violet filter Viking images are displayed in the blue channel. This image is part of the digital color composite assembled and discussed by McEwen *et al.* (1993).

FIG. 2. (a) Color composite of three selected endmember fraction images from linear spectral mixture modeling. The endmembers in the mixture model are spectra from South Acidalia (SA), Arabia (AR), Sinus Meridiani (SM), and Deucalionis Regio (DR). This color composite shows the Arabia fraction in red, the Sinus Meridiani fraction in green, and the Deucalionis fraction in blue. (b) Color-coded map of the spectral varieties in the 1988 telescopic spectral image. The map was produced by supervised classification of the spectral shapes using an artificial neural network. The spectral types are: SA = Acidalia Planitia; CL = optically thin atmospheric condensates; CY = Chryse; AR = Arabia; SM = hematite rich soil no. 1; SM2 = hematite rich soil no. 2.; DR = Deucalionis Regio no. 1; DR2 = Deucalionis Regio no. 2. The three remaining classes have no geological relevance: U = unclassified; L = limb effects; and S = sky/background. These figures were projected onto cylindrical coordinates using the procedure described by Pierazzo and Singer (1993). The fringes at the top of the image may be unreliable due to limb effects.

FIG. 7. Generalized thermal inertia map of Arabia–Deucalionis region of Mars, illustrating the possible occurrence of distinct thermophysical units in the soils concentric to Arabia. *Unit* 1, interpreted as loose dust, has a Kieffer-model thermal inertia of 100 ± 20 (2.5 ± 0.35). *Unit* 2, with thermal inertia = 170 ± 10 (4.0 ± 0.2), is interpreted as a slightly crusted soil; *Unit* 3 is somewhat more indurated with thermal inertia = 210 ± 20 (4.9 ± 0.4). *Units* 4 (thermal inertia = 280 ± 50 (6.6 ± 1.1)) and 5 (thermal inertia = 370 ± 50 (8.8 ± 1.2)) probably cannot be fit into this scheme, and may consist of crusts, sands, rocks, and other materials. *Unit* 6, for thermal inertias > 420 (10.0), includes most regions of high rock abundance (Christensen 1986a). Adjusted for $\tau = 0.4$ conditions according to Haberle and Jakosky (1991), all of these thermal inertias would be lower. *Unit* 1 would be about 30 ± 20; *Unit* 2, 90 ± 10; *Unit* 3, 130 ± 20; *Unit* 4, 180 ± 50; *Unit* 5, 260 ± 50; and *Unit* 6, >300. This figure is our interpretation of the Arabia-concentric indurated dust deposit ideas described by Christensen and Malin (1988) and Christensen and Moore (1992). The data used here are the same as in Fig. 5.

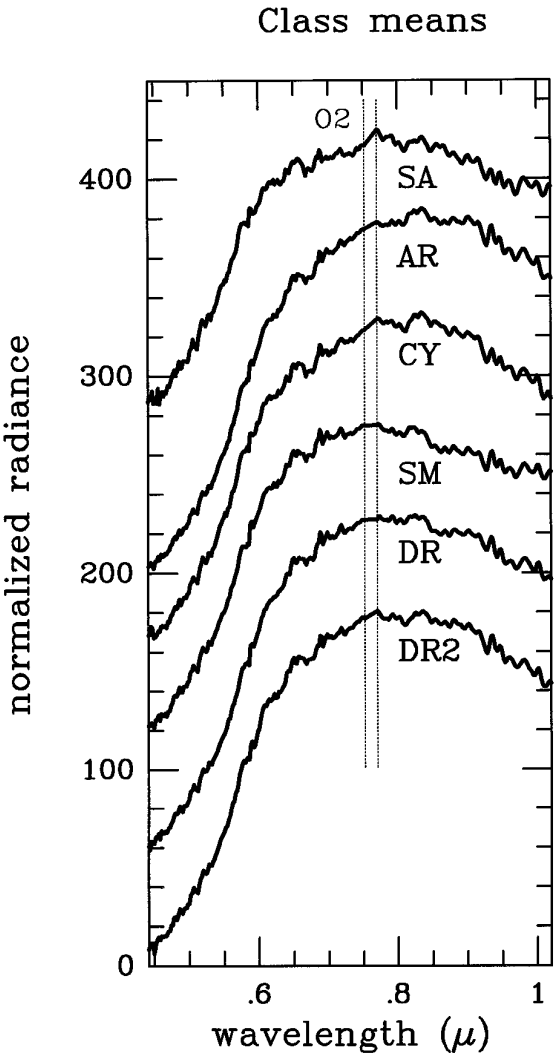

FIG. 3. Mean spectra of the classes in Fig. 2b for the spectral units considered in this study. The curves are offset for better viewing. Interpretation is based on broad spectral features and continuum shapes. These spectra exhibit subtle but real differences on the order of a few percent of the data value range, which are enhanced in ratios and are important for their interpretation.

pyroxene Fe^{2+} absorptions is difficult from our observations, however, because the data do not extend to long enough wavelengths to define the complete band. An additional complication is the possibility of Fe^{3+} crystal-field absorptions from crystalline ferric oxide minerals, ranging from about 0.86 to about 0.93 μm, depending on composition. Lastly, imperfect correction for telluric water absorptions around 0.82 and 0.94 μm adds "noise" to these spectra (see Merényi *et al.* (1996)). We stress that none of these factors negate the fact that most of the spectral uniqueness of Deucalionis Regio occurs in the 0.8–1.0 μm spectral region. They do, however, complicate specific compositional interpretations. If we assume a modest Ca pyroxene (an augite, with a band near 0.93–0.97 μm), and based on the ratio spectra presented in Fig. 4, it appears that Deucalionis may have less pyroxene than Sinus Meridiani because the ratio spectrum DR/SM is convex upwards in the 0.9–0.95 μm region. In contrast, Deucalionis may have more pyroxene than Arabia, because the ratio spectrum DR/AR is concave upwards in the 0.9–0.95 μm region. This would make geologic sense. Many low-latitude regions such as Sinus Meridiani with relatively unweathered low-albedo surface cover are known to contain substantial pyroxene (presumably derived from basaltic crust) (e.g., Miller and Singer 1993; Singer and McSween 1993; Mustard *et al.* 1993). Arabia, one of the classic bright heavily weath-

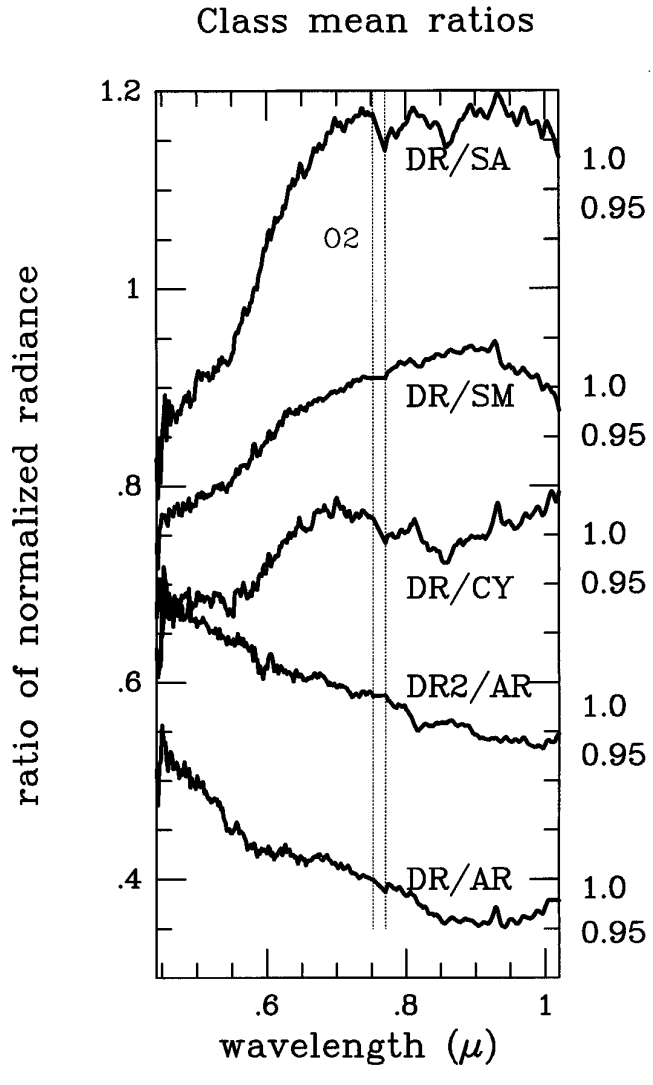

FIG. 4. Ratios of the mean Deucalionis Regio spectrum (DR) to the mean spectra of other spectral units in this study. The curves are offset for clarity. Noticeable are the variation in the 0.53 μm Fe^{3+} band depth and variation in the behavior of the broad Fe^{2+} band centered around 0.86 μm. See text for more discussion.

ered soil units, contains much less pyroxene (e.g., McCord *et al.* 1982b). Deucalionis Regio, a region with intermediate albedo, might very reasonably have a multicomponent soil containing basalt fragments (including pyroxenes) intimately mixed with more-weathered materials.

The unit DR2, originally part of the area that the linear mixture model mapped as ''Deucalionis Regio material'' was identified by the classification of spectral shapes (Fig. 2b). DR2 seems to have different spectral properties than DR. The ratio of DR2 to Arabia in Fig. 4 is nearly linear, with a blue continuum slope. The lack of specific absorption bands implies that the mineralogy of these two regions is similar. The difference in spectral slope might be caused by physical differences affecting scattering, and/or greater Fe^{3+} content in Arabia, in the form of poorly crystalline or nanophase grains.

3. SURFACE PHYSICAL PROPERTIES

3.1. Data and Usage

The discussions above indicate that the optical surface of Deucalionis Regio is different from its surrounding regions. These regions have other surface layer characteristics which make them different from each other. Although the following interpretations are our own, this section relies almost entirely on data and model-dependent results presented by others. Lambert albedos are from the Viking Infrared Thermal Mapper (IRTM) broadband (0.3–3.0 μm) observations compiled by Pleskot and Miner (1981) and Christensen (1988). Thermal inertia and rock abundance maps are derived from IRTM thermal infrared observations compiled by Christensen (1986a), Christensen and Malin (1988), and illustrated by Christensen and Moore (1992). Occurrence of localized dust storms is from the listings of Peterfreund (1985). Discussion of surface wind shear stress comes from figures derived by Skypeck (1989) and Greeley *et al.* (1993) from the general circulation models of Pollack *et al.* (1981, 1990). The reader is referred to these works to see how the data and models were selected and interpreted by these authors.

3.2. IRTM-Derived Results

The albedo, modeled rock abundance, thermal inertia, and interpreted effective particle sizes for Deucalionis Regio, Arabia, Acidalia, Sinus Meridiani, and Oxia, are listed in Table I. Thermal inertia (the square root of the product of bulk density, specific heat, and thermal conductivity) provides a means to estimate the effective particle size of materials at Martian atmospheric pressures sensed by thermal infrared radiometry (Neugebauer *et al.* 1971; Edgett and Christensen 1991). Thermal inertias are expressed here in units of J m^{-2} $s^{-0.5}$ K^{-1}. Thermal inertias in units of 10^{-3} cal cm^{-2} $s^{-0.5}$ K^{-1} were used in nearly all reports of Viking IRTM results between 1976 and 1990, thus these too are given here in parentheses following the S.I. values. There has recently been considerable discussion of atmospheric corrections for the models used to calculate thermal inertia (Haberle and Jakosky 1991; Paige *et al.* 1994; Edgett and Christensen 1994). Here we present thermal inertias derived using the thermal model of Kieffer *et al.* (1977). The Kieffer-model thermal inertias represent upper limits. Thermal inertias for dust opacity conditions of $\tau = 0.4$ modeled by Haberle and Jakosky (1991) are probably closer to the actual thermal inertia, thus in Table I we present both the Kieffer-model thermal inertias and values estimated for the $\tau = 0.4$ conditions using the work of Haberle and Jakosky (1991). Interpretation of particle size from thermal inertia is complicated by the uncertainty in atmospheric opacity effects; here (Table I) we use the $\tau = 0.4$ thermal inertias and interpret particle size as discussed by Edgett and Christensen (1991, 1994).

The spatial variation of thermal inertia is illustrated in Fig. 5. The IRTM-derived albedos are shown in Fig. 6. The IRTM-derived results for Arabia, Oxia, Acidalia, and Sinus Meridiani (Table I) have been discussed by previous authors (Kieffer *et al.* 1977, 1981; Christensen 1986a, 1986b, 1988; Presley and Arvidson 1988; Arvidson *et al.* 1989; Christensen and Moore 1992). Their interpretations suggest that Arabia is largely mantled by $\leq$1 m of fine, bright dust, Sinus Meridiani is mostly covered with deposits of dark, presumably mafic sand, and Acidalia has variable spatial coverage of sand and coarser materials, including rocks. However, the physical nature of the surface layer in Oxia is somewhat problematical: the Dark Red unit might result from mixing of Dark Gray sand and Bright Red dust (Christensen and Malin 1993) or from erosion and exposure of crusted, Bright Red dust (Presley and Arvidson 1988; Christensen and Malin 1988).

Deucalionis Regio is different from the other nearby regions in Table I. It has an intermediate albedo that does not vary much over the region. It has among the lowest rock abundances measured anywhere on the planet. Although a simplistic view, observation has generally shown that locations on Mars which have a low rock abundance are regions of modern aeolian sediment deposition (Christensen 1986a; Christensen and Malin 1993). The regional thermal inertia results imply that the soils in Deucalionis Regio have an IRTM-derived effective particle size on the order of 100 $\pm$ 50 μm, or silt to fine sand. The effective particle size determined for Deucalionis Regio might be a measure of true average grain size, but it can also indicate that the actual particle size is smaller and that grains have been bonded to some degree, or that the soil is a multicomponent mixture of abundant fines and moderate amounts of coarser grains (e.g., Jakosky and Christensen 1986; Christensen and Moore 1992).

TABLE I
Comparison of Physical Characteristics of Regions Considered in This Study

	Arabia	Oxia[a]	Deucalionis	S. Meridiani	Acidalia
Albedo[b]	0.21–0.23	0.17–0.19	0.18–0.20	0.08–0.12	0.05–0.12
Rock abundance[c]	≤8%	4–10%	<5%	≤10%	5–20%
Thermal inertia					
Kieffer model[d]	80–130	150–270	190–270	290–380	420–670
	(2.0–3.0)	(3.5–6.5)	(4.5–6.5)	(7.0–9.0)	(10.0–16.0)
Haberle–Jakosky[e]	20–60	70–170	110–180	200–250	300–480
	(0.5–1.4)	(1.7–4.1)	(2.6–4.2)	(4.7–6.0)	(7.2–11.5)
Effective particle size[f]					
Kieffer model	30–60	80–300	125–300	320–670	850–5000
Haberle–Jakosky	5–20	25–100	50–100	150–250	400–1100
Grain size class[g]	clay to silt	silt to very fine sand	silt to very fine sand	very fine to medium sand	medium to coarse sand

[a] "Dark Red" unit of Arvidson *et al.* (1989) only.
[b] From digital copy of Fig. 2 in Christensen (1988).
[c] From digital copy of Fig. 5 in Christensen (1986a).
[d] Single-point thermal inertias (units of J m^{-2} $s^{-0.5}$ K^{-1}, and 10^{-3} cal cm^{-2} $s^{-0.5}$ K^{-1} in parentheses) computed using the standard Kieffer *et al.* (1977) thermal model. From digital copy of Fig. 5 in Christensen and Moore (1992).
[e] Calculated from Kieffer model inertias using Fig. 13 in Haberle and Jakosky (1991) for $\tau = 0.4$ conditions.
[f] From Fig. 2 in Edgett and Christensen (1991), units in μm.
[g] For the $\tau = 0.4$ case, as discussed by Edgett and Christensen (1994); Wentworth (1922) classification scheme.

3.3. Aeolian Considerations

On Mars, surfaces composed of particles with diameters on the order of 115 ± 50 μm are susceptible to the lowest threshold friction speeds (1.9 to 2.1 m/sec) required to initiate particle motion (Iversen and White 1982). Thus, the soils in Deucalionis Regio would appear from thermal inertia to be within the range most susceptible to aeolian activity (100 ± 50 μm). Such grains are small enough (<210 μm), however, that once set in motion they might be expected to go into short-term suspension (Edgett and Christensen 1994, Fig. 8). If Deucalionis Regio is composed of loose, ≃100 μm particles, and if the winds in this region are strong enough to entrain these particles, then there should be evidence of this motion. Such evidence would be (*a*) the presence of dunes, (*b*) spatial and/or temporal variations in surface albedo, or (*c*) local dust storms indicating active suspension and removal of dust.

The shear stress maps presented by Greeley *et al.* (1993) indicate the relative differences in wind speed in different regions. It has been noted previously by Zimbelman and Kieffer (1979) and Christensen (1986b) that there is an excellent correlation between regions of perennially low wind strength and the occurrence of vast dust and silt deposits in Arabia and the Tharsis and Elysium volcanic regions (not shown in Fig. 1). There is likewise a similar correlation between the occurrence of strong winds and sand- and rock-covered regions like Acidalia (Skypeck 1989, Greeley *et al.* 1993). In general, the wind shear figures indicate that Deucalionis Regio has moderate winds that tend to be stronger than those in Sinus Sabaeus to the north but weaker than winds in Pandorae Fretum to the south. Sinus Sabaeus and Pandorae Fretum are both regions of observed aeolian activity. Pandorae Fretum was considered by Slipher (1962, p. 11) to be one of the most active regions on Mars, undergoing striking albedo changes on the time scale of months or years (Martin *et al.* 1992). In contrast, Sinus Sabaeus is one of the most persistent dark features on Mars (Slipher 1962, p. 12). Low albedo features like Sinus Sabaeus are generally considered to be maintained by saltation of dark sand grains which keep the surface swept clean of Bright Red dust (cf., Thomas 1984; Singer *et al.* 1984; Lee 1986; Christensen 1988). Given that Sinus Sabaeus and Pandorae Fretum apparently have active wind regimes, it seems likely that Deucalionis Regio must also be subjected to winds that are at least strong enough to move sediment. However, the albedo of Deucalionis Regio appears to change little over time (see McCord *et al.* 1982a, Fig. 10).

Localized dust storms are closely related to the action of wind upon the surface that is actually enveloped by the storm, whereas regional and global storms may obscure areas larger than those affected at the surface. Figure 6 shows the center points of local dust storms that were observed in the vicinity of Deucalionis Regio between 1873 and 1980 (Peterfreund 1985). None of these storms occurred directly within Deucalionis Regio, although several occurred along its margins. (We note, however, that dust clouds from regional and global storms have sometimes obscured Deucalionis Regio from view (Antoniadi 1930; Martin and Zurek 1993)). We conclude from Fig. 6 that

few, if any, dust storms have originated in Deucalionis Regio over the past ≃120 years.

The soils of Deucalionis Regio might not contain very much sand. All known sand deposits on Mars have low albedos (e.g., Cutts and Smith 1973; Thomas and Weitz 1989; Geissler *et al.* 1990). The surface materials in Deucalionis Regio, though having IRTM-derived effective particle sizes largely in the very fine sand range, do not have a low albedo. Thus, if this intermediate-albedo region is actually covered with sand, then it would have a composition that is different than any previously identified sand deposits on Mars. If instead the soil is composed of a loose mixture of dark sand and bright weathered dust, it might be expected that, over time, wind acting upon this mixture would sort and separate the sand and dust. Such sorting would likely create low-albedo sand drifts and raise clouds of dust (e.g., Daniel 1936), neither of which have been observed. We therefore conclude that the soil comprising most of the Deucalionis Regio surface layer is immobile.

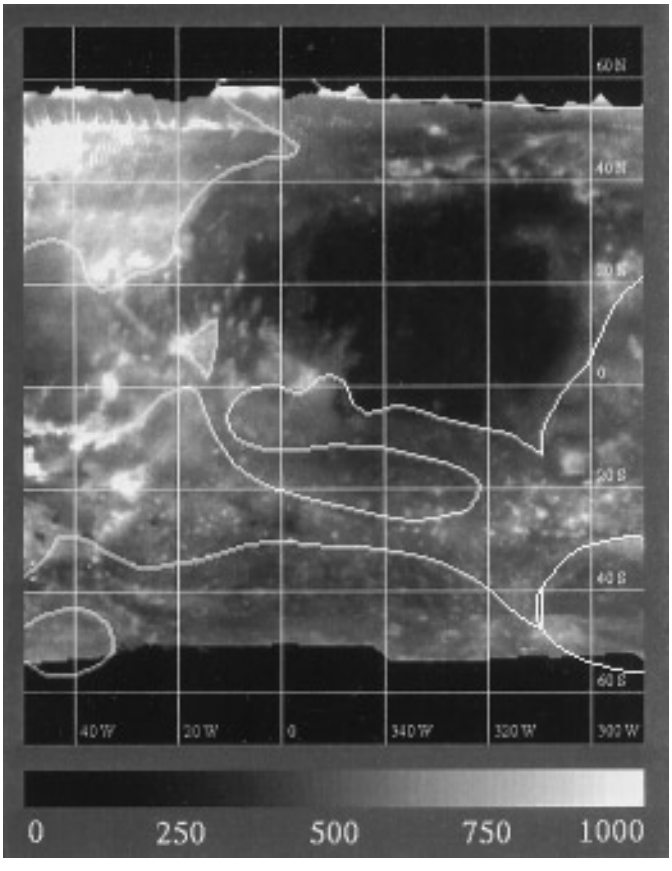

FIG. 5. Thermal inertia map of the area around Deucalionis Regio. Thermal inertias were computed using the Kieffer *et al.* (1977) thermal model and represent upper limits. The relative differences are important and would remain the same even if atmospheric corrections were applied. Thermal inertias shown here are in units of J m^{-2} $s^{-0.5}$ K^{-1}. To convert to units of 10^{-3} cal cm^{-2} $sec^{-0.5}$ K^{-1}, divide by 41.84. A thermal inertia of 250 in the diagram above corresponds to a thermal inertia of 160 when corrected for the $\tau = 0.4$ dust opacity conditions as per Haberle and Jakosky (1991). Likewise, a thermal inertia of 500 above would become 370. This is a portion of a map provided by P. R. Christensen derived from Viking Infrared Thermal Mapper (IRTM) data (Christensen and Malin 1988; Christensen and Moore 1992).

FIG. 6. Occurrences of local dust storms between 1873 and 1980. Note that no storms were centered on Deucalionis Regio. Albedo data are derived from the Viking IRTM (Pleskot and Miner 1981; Christensen 1988). Storm locations were listed by Peterfreund (1985).

4. DISCUSSION

Soil surfaces might become generally stable in an arid aeolian environment if the surface is (a) armored with very dense or large particles, (b) covered with large roughness elements such as rocks protruding into the air flow, or (c) consolidated or crusted (Chepil and Woodruff 1963). Rock abundance in Deucalionis Regio is apparently very low, and it is unlikely that the surface is armored by dense particles, because typical dense minerals such as magnetite are dark. Thus, the remaining explanations appear to be (1) armoring by particles smaller than 10 cm (the size of Christensen's (1986a) ''rocks''), and (2) a crusted or otherwise consolidated soil composed of particles that are

generally smaller than the IRTM-derived effective particle size (100 ± 50 μm).

As on Earth, an armor or stone pavement would consist of a layer of coarse particles one or two grains thick covering a soil composed of finer grains (Cooke and Warren 1973, p. 120). Terrestrial stone pavements usually result from a combination of processes requiring the presence or occassional occurrence of liquid or frozen water at or near the surface (Cooke and Warren 1973, pp. 124–129). However, wind might sometimes act alone to sort materials and produce an armor by removal of surface fines via saltation and impact-induced suspension (Chepil 1950). If the entire Deucalionis region is armored, we would expect the surface grains to be coarser than sand (because the surface is not dark and covered by dunes) but finer than the 10 cm rock abundance constraint. Such grains could be on the order of 5 cm in size, which could lead to the estimated effective particle size of 100 ± 50 μm only if the underlying soil was very fine ($\ll 50$ μm). The maximum spacing between armoring pebbles is generally estimated by $d = D/\tan \phi$, in which d is the spacing between pebbles of diameter D, and ϕ is the impact angle of a saltating grain. Assuming saltation impact angles of about $10° \pm 4°$ (e.g., White 1979), loose grains $\simeq 5$ cm in height would need to be spaced no more than 15 cm apart to effectively protect the surface from further aeolian erosion. The armoring particles, or at least their optical surface, would have to be significantly weathered to produce the observed spectral properties of Deucalionis Regio.

We favor an alternative hypothesis, that the soils of Deucalionis Regio are cemented. The stabilization of these materials may resemble that in the soils seen at the Viking lander sites which were cemented by salts. To stabilize the soil, a crust need only be a millimeter to two thick (Chepil and Woodruff 1963), but could be several centimeters (or more) in thickness, similar to the crusts observed at the Viking lander sites (e.g., Moore *et al.* 1987). The depth of induration cannot be determined from the available data. The possibility that Mars might have regional-scale exposures of crusted soil was proposed by Jakosky and Christensen (1986). Singer *et al.* (1984) suggested this might be true in Lunae Planum, and several authors have proposed that the Dark Red soils in Oxia and Chryse may also be crusted (e.g., Kieffer *et al.* 1981; Presley and Arvidson 1988; Arvidson *et al.* 1989). Finally, Christensen and Moore (1992) suggested that large portions of the Martian southern hemisphere (e.g., Noachis, where albedos and thermal inertias tend to have average or intermediate values) may also consist of crusted soils. Figure 7 shows that there seem to be distinct concentric units or zones of approximately uniform thermal inertia surrounding Arabia. Arabia is considered to be largely mantled by unconsolidated, bright dust (Christensen 1986b). Christensen and Moore (1992, p. 723) have suggested that the zones concentric to Arabia might be older layers of dust that were deposited from aeolian suspension some time in the past. These dust deposits would have subsequently become indurated, and later re-exposed by aeolian erosion. This hypothesis assumes that dust once covered a much larger area than it does today, an assumption that probably cannot be tested with available data. However, if this model is correct, then Deucalionis Regio would be the southernmost extent of these older, stabilized dust layers. The model would also suggest that crusted material underlies the low-albedo Sinus Sabaeus, an observation probably consistent with the presence of distinct intermediate-albedo surfaces within and partly covered by dark, sandy materials (Fig. 1). Further, this model is consistent with the observation that Oxia and Deucalionis Regio have similar thermal properties (Fig. 7).

Our analyses show that spectral and physical properties similar to those of Deucalionis Regio are also spatially correlated in other regions, such as Oxia and western Noachis. In Fig. 7, the thermal inertia zones that might be interpreted as crusted surfaces (units #2 and #3) coincide with Deucalionis, Oxia, and western Noachis. These areas, together with Chryse (another area of proposed crusted soil), have significant spectral contributions from the Deucalionis-type units (both DR and DR2). Such large-scale spatial correlations suggest that the composition and the physical structure of the soil may be genetically related over extensive areas on the surface of Mars. There is, however, no hard evidence from the data presently available to prove that this is more than a coincidence. Perhaps the proposed crusted soil contains sediments deposited in an earlier epoch, genetically different from the current aeolian global dust. Additionally, both the albedo and spectral properties of the DR units are consistent with the possibility of a complex, multicomponent soil, with contributions from dark, relatively unaltered phases, possibly including pyroxene-bearing crust as well as brighter, weathered (or otherwise altered) material. This opens the question of which transport mechanism(s) were responsible for deposition of surface material(s) currently seen at the surface of Deucalionis Regio. Very fine-grained material derived from nearly anywhere on the planet could have been deposited from aeolian suspension, as previously suggested by many researchers. This mechanism is especially suitable for heavily weathered materials, which tend to naturally produce dust-sized particles (e.g., Allen *et al.* 1981; Singer 1982). The possibility of *in situ* alteration of at least some weathered soil components cannot yet be ruled out, however. For coarser-grained material now incorporated into a composite soil (such as pyroxene-bearing basalt fragments) transportation over shorter distances by saltation seems more probable. We predict that in at least some cases this coarser soil component may be representative of the local composition of the martian crust and/or

material derived from the adjacent low-albedo regions. Whatever their origin(s), all components of Deucalionis-like soils might presently be stabilized by crusts/induration or some other form of immobilization. This type of stabilized soil deposit, perhaps cemented by salts, might actually be common on Mars. Previous work of McCord *et al.* (1982a) and Christensen and Moore (1992) suggested that crusted soils might be common in the southern hemisphere.

The probability that soils comprising the intermediate-albedo Deucalionis Regio are immobile and possibly crusted can be tested by specific observations from future Mars-orbiting spacecraft. The key questions are: (a) is the soil immobile, and if so, is it armored or crusted, (b) do salts comprise the soil, (c) what mineral causes the observed different spectral character of the region, and (d) is the surface of Deucalionis Regio truly unique or simply a good example of a more extensive soil type in the southern hemisphere (cf. western Noachis)? High spatial resolution images in visible wavelengths from a lander or from a Mars-orbiting spacecraft could provide continued monitoring of the apparent immobility of the soil (i.e., look for local dust storms). A Mars Observer-class thermal emission spectrometer should provide key observations for distinguishing between the armor and crust models, and also for the detection of salts down to 2–8% concentration level depending on soil physical properties (Wenrich and Christensen, 1994). Complemented with observations from a visible and near-infrared spectrometer and a gamma ray spectrometer, detailed information for the mineralogical makeup of Deucalionis could be obtained.

5. CONCLUSIONS

Two independent analyses of a visible/near-infrared telescopic spectral image of Mars obtained during the 1988 opposition indicate that the equatorial classical albedo feature Deucalionis Regio is different in color and composition relative to the usual Bright Red, Dark Red, and Dark Gray Viking color units commonly associated with Martian albedo regions. The spectral observations suggest that this soil has a composition that is different from the materials in nearby regions such as Arabia, Acidalia, Meridiani, and probably Oxia. A combination of observations, including thermal inertia, rock abundance, and effective particle size estimated from Viking IRTM results; observations of localized dust storms for the period 1873–1980; and surface wind shear stress derived from general circulation models; suggest that the soils in Deucalionis Regio are relatively fine-grained with few coarse materials such as sand, pebbles, or cobbles, and that these soils are probably immobile despite windy conditions. Deucalionis Regio is apparently a regional exposure of crusted or indurated soil. We predict that a Mars Observer-class thermal emission spectrometer will show the presence of crust-forming salts in the soils of this region, and that a gamma ray spectrometer will measure high concentrations of salt-forming elements. We found spatial correlation between similar spectral and physical properties as those of Deucalionis Regio, in other extensive areas, most notably in Oxia and western Noachis, which may suggest a genetic tie between these properties.

ACKNOWLEDGMENTS

The authors are grateful to P. R. Christensen for providing his results of the IRTM data analysis in digital form. Thorough and constructive reviews by J. F. Mustard and J. M. Moore greatly helped improve the original manuscript. We appreciate helpful discussions with M. A. Presley, M. L. Wenrich, M. C. Malin, R. G. Strom, and S. K. Croft. Contributions to this work by J. S. Miller and by NASA Space Grant Intern Trevor Laing are much appreciated. We thank J. B. Adams and M. O. Smith for providing the linear mixture model software. For spectral classification, the artificial neural network simulation package "NeuralWorks Professional II," by NeuralWare, Inc., was used. This project was partially supported by NASA Grant NAGW-1059 and by the University of Arizona Planetary Image Research Laboratory. KSE was supported by an Educational Supplement to NASA Grant NAGW-943. The computing facilities of the Lunar and Planetary Laboratory and the Planetary Image Research Laboratory at the University of Arizona and the Khoros image processing package (Rasure and Young, 1992) were used for the image analysis work.

REFERENCES

Adams, J. B. 1975. Interpretation of visible and near-infrared diffuse reflectance spectra of pyroxenes and other rock-forming minerals. In *Infrared and Raman Spectroscopy of Lunar and Terrestrial Minerals*, (C. Karr, Jr., Ed.), pp. 91–116. Academic Press, San Diego.

Allen, C. C., J. L. Gooding, M. Jercinovic, and K. Keil 1981. Altered basaltic glass: Terrestrial analog to the soil of Mars. *Icarus* **45,** 347–369.

Antoniadi, E. M. 1930. *La Planète Mars.* Hermann, Paris.

Arvidson, R. E., E. A. Guiness, M. A. Dale-Bannister, J. B. Adams, M. O. Smith, P. R. Christensen, and R. B. Singer 1989. Nature and distribution of surficial deposits in Chryse Planitia and vicinity, Mars. *J. Geophys. Res.* **94,** 1573–1587.

Baum, W. A., R. L. Millis, S. E. Jones, and L. J. Martin 1970. The International Planetary Patrol Program. *Icarus* **12,** 435–439.

Burns, R. G. 1970. *Mineralogical Applications of Crystal Field Theory.* Cambridge Univ. Press, Cambridge, UK.

Chepil, W. S. 1950. Properties of soil which influence wind erosion. I. The governing principle of surface roughness. *Soil Sci.* **69,** 149–162.

Chepil, W. S., and N. P. Woodruff 1963. The physics of wind erosion and its control. *Adv. Agron.* **15,** 211–302.

Christensen, P. R. 1986a. The spatial distribution of rocks on Mars. *Icarus* **68,** 217–238.

Christensen, P. R. 1986b. Regional dust deposits on Mars: Physical properties, age, and history. *J. Geophys. Res.* **91,** 3533–3546.

Christensen, P. R. 1988. Global albedo variations on Mars: Implications for active aeolian transport, deposition, and erosion. *J. Geophys. Res.* **93,** 7611–7624.

Christensen, P. R., and M. C. Malin 1988. High resolution thermal imaging of Mars. *Lunar Planet. Sci.* **19,** 180–181. [Abstract]

Christensen, P. R., and H. J. Moore 1992. The martian surface layer. In *Mars* (H. H. Kieffer, B. M. Jakosky, C. W. Snyder, and M. S. Matthews, Eds.), pp. 686–729. Univ. of Arizona Press, Tucson.

Christensen, P. R., and M. C. Malin 1993. A simple model of clastic sediments on Mars. *Lunar Planet. Sci.* **24,** 285–286. [Abstract]

Cooke, R. U., and A. W. Warren 1973. *Geomorphology in Deserts.* Univ. of California Press, Los Angeles.

Cutts, J. A., and R. S. U. Smith 1973. Eolian deposits and dunes on Mars. *J. Geophys. Res.* **78,** 4139–4154.

Daniel, H. A. 1936. The physical changes in soils of the southern high plains due to cropping and wind erosion and the relation between the (sand + silt)/clay ratios in these soils. *J. Amer. Soc. Agron.* **28,** 570–580.

Edgett, K. S., and P. R. Christensen 1991. The particle size of martian aeolian dunes. *J. Geophys. Res.* **96,** 22,765–22,776.

Edgett, K. S., and P. R. Christensen 1994. Mars aeolian sand: Regional variations among dark-hued crater floor features. *J. Geophys. Res.* **99,** 1997–2018.

Geissler, P. E., R. B. Singer, and B. K. Lucchitta 1990. Dark materials in Valles Marineris: Indications of the style of volcanism and magmatism on Mars. *J. Geophys. Res.* **95,** 14,399–14,413.

Geissler, P. E., R. B. Singer, G. Komatsu, S. Murchie, and J. F. Mustard 1993. An unusual spectral unit in west Candor Chasma: Evidence for aqueous or hydrothermal alteration in the martian canyons. *Icarus* **106,** 380–391.

Greeley, R., A. Skypeck, and J. B. Pollack 1993. Martian aeolian features and deposits: Comparisons with general circulation model results. *J. Geophys. Res.* **98,** 3183–3196.

Haberle, R. M., and B. M. Jakosky 1991. Atmospheric effects on the remote determination of thermal inertia on Mars. *Icarus* **90,** 187–204.

Iversen, J. D., and B. R. White 1982. Saltation threshold on Earth, Mars, and Venus. *Sedimentology* **29,** 111–119.

Jakosky, B. M., and P. R. Christensen 1986. Global duricrust on Mars: Analysis of remote-sensing data. *J. Geophys. Res.* **91,** 3547–3559.

Kieffer, H. H., T. Z. Martin, A. R. Peterfreund, B. M. Jakosky, E. D. Miner, and F. D. Palluconi 1977. Thermal and albedo mapping of Mars during the Viking primary mission. *J. Geophys. Res.* **82,** 4249–4292.

Kieffer, H. H., P. A. Davis, and L. A. Soderblom 1981. Mars' global properties: Maps and applications. *Lunar Planet. Sci. B* **12,** 1395–1417.

Lee, S. W. 1986. IRTM observations of Syrtis Major: An active aeolian environment. In *Reports of the Planetary Geology and Geophysics Program—1985,* NASA Tech. Memo. TM 88383, pp. 532–534.

Martin, L. J., P. B. James, A. Dollfus, K. Iwasaki, and J. D. Beish 1992. Telescopic observations: Visual, photographic, polarimetric. In *Mars* (H. H. Kieffer, B. M. Jakosky, C. W. Snyder, and M. S. Matthews, Eds.) pp. 34–70. Univ. of Arizona Press, Tucson.

Martin, L. J., and R. W. Zurek 1993. An analysis of the history of dust activity on Mars. *J. Geophys. Res.* **98,** 3221–3246.

McCord, T. B., R. B. Singer, B. R. Hawke, J. B. Adams, D. L. Evans, J. W. Head, P. J. Mouginis-Mark, C. M. Pieters, R. L. Huguenin, and S. H. Zisk 1982a. Mars: Definition and characterization of global surface units with emphasis on composition. *J. Geophys. Res.* **87,** 10,129–10,148.

McCord, T. B., R. N. Clark, and R. B. Singer 1982b. Mars: Near-infrared reflectance spectra of surface regions and compositional implication. *J. Geophys. Res.* **87,** 3021–3032.

McEwen, A. S., L. A. Soderblom, T. L. Becker, E. M. Lee, and R. M. Batson 1993. Global color views of Mars. In *Mars: Past, Present, and Future Results from the MSATT Program* (R. M. Haberle, Ed.) LPI Tech. Rept. 93-06, Part 1, p. 29. Lunar and Planetary Institute, Houston.

Merényi, E., J. S. Miller, and R. B. Singer 1992. Compositional variations on the surface of Mars: Mixing model analysis from a telescopic spectral image. *Lunar Planet. Sci.* **23,** 897–898. [Abstract]

Merényi, E., R. B. Singer, and J. S. Miller 1996. Mapping of spectral variations on the surface of Mars from high spectral resolution telescopic images. *Icarus,* **124,** 280–295.

Miller, J. S., and R. B. Singer 1993. Analysis of pyroxene absorptions observed in martian dark regions. *Lunar Planet. Sci.* **24,** 989–990. [Abstract]

Moore, H. J., R. M. Hutton, G. D. Clow, and C. R. Spitzer 1987. *Physical Properties of the Surface Materials at the Viking Landing Sites on Mars.* U.S. Geol. Surv. Prof. Paper **1389**.

Morris, R. V., and H. V. Lauer 1990. Matrix effects for reflectivity spectra of dispersed nanophase (superparamagnetic) hematite with application to martian spectral data. *J. Geophys. Res.* **95,** 5101–5109.

Murchie, S. L., J. F. Mustard, J. L. Bishop, J. W. Head, C. M. Pieters, and S. Erard 1993. Spatial variations in the spectral properties of bright regions on Mars. *Icarus* **105,** 454–468.

Murray, B. C., L. A. Soderblom, R. P. Sharp, and J. A. Cutts 1971. The surface of Mars. 1. Cratered terrains. *J. Geophys. Res.* **76,** 313–330.

Mustard, J. F., S. L. Murchie, and S. Erard 1993. Composition of weakly altered martian crust. *Lunar Planet. Sci.* **24,** 1039–1040. [Abstract]

Neugebauer, G., G. Münch, H. Kieffer, S. C. Chase, Jr., and E. Miner 1971. Mariner 1969 infrared radiometer results: Temperatures and thermal properties of the martian surface. *Astron. J.* **76,** 719–728.

Paige, D. A., J. E. Bachman, and K. D. Keegan 1994. Thermal and albedo mapping of the polar regions of Mars using Viking thermal mapper observations. 1. North polar region. *J. Geophys. Res.* **99,** 25,969–25,991.

Peterfreund, A. R. 1985. *Contemporary Aeolian Processes on Mars: Local Dust Storms.* Ph.D. Dissertation, Arizona State University, Tempe.

Pierazzo, E., and R. B. Singer 1993. Wavelength dependence of limb-darkening of Mars from visible and near-IR telescopic spectral imaging. *Lunar Planet. Sci.* **24,** 1139–1140. [Abstract]

Pleskot, L. K., and E. D. Miner 1981. Time variability of martian bolometric albedo. *Icarus* **45,** 179–201.

Pollack, J. B., C. B. Leovy, P. W. Greiman, and Y. Mintz 1981. A martian general circulation experiment with large topography. *J. Atmos. Sci.* **38,** 3–29.

Pollack, J. B., R. M. Haberle, J. Schaeffer, and H. Lee 1990. Simulations of the general circulation of the martian atmosphere. 1. Polar processes. *J. Geophys. Res.* **95,** 1447–1473.

Presley, M. A., and R. E. Arvidson 1988. Nature and origin of materials exposed in the Oxia Palus—Western Arabia—Sinus Meridiani region, Mars. *Icarus* **75,** 499–517.

Rasure, J., and M. Young 1992. An open environment for image processing software development. In *Proceedings of the SPIE/IS&T Symposium in Electronic Imaging, February 14, 1992,* Vol. 1659.

Singer, R. B., and T. B. McCord 1979. Mars: Large scale mixing of bright and dark surface materials and implications for analysis of spectral reflectance. *Lunar Planet. Sci.* **10,** 1835–1848.

Singer, R. B. 1982. Spectral evidence for the mineralogy of high-albedo soils and dust on Mars. *J. Geophys. Res.* **87,** 10,159–10,168.

Singer, R. B., E. Cloutis, T. L. Roush, P. J. Mouginis-Mark, B. R. Hawke, and P. R. Christensen 1984. Multispectral analysis of the Kasei Vallis—Lunae Planum region of Mars. *Lunar Planet. Sci.* **25,** 794–795. [Abstract]

Singer, R. B., J. S. Miller, K. W. Wells, and E. S. Bus 1990. Visible and near-IR spectral imaging of Mars during the 1988 opposition. *Lunar Planet. Sci.* **21,** 1164–1165. [Abstract]

SINGER, R. B., AND J. S. MILLER 1991. Evidence for crystalline hematite as an accessory phase in martian soils. In *Workshop on the Mars Surface and Atmosphere Through Time* (R. M. Haberle, Ed.), pp. 134–135. LPI Tech. Rept. 92-02, Lunar and Planetary Institute, Houston. [Abstract]

SINGER, R. B., AND H. Y. MCSWEEN 1993. The composition of the igneous martian crust: Evidence from remote sensing and SNC meteorites. In *Resources of Near-Earth Space* (J. Lewis, M. S. Matthews, and M. L. Guerrieri, Eds.) pp. 709–736. Univ. of Arizona Press, Tucson.

SKYPECK, A. P. 1989. *Comparison of Mars General Circulation Model with Aeolian Features and Deposits.* M. S. Thesis, Arizona State University, Tempe.

SLIPHER, E. C. 1962. *The Photographic Story of Mars.* Sky Publishing, Cambridge, MA/Northland Press, Flagstaff, AZ.

THOMAS, P. 1984. Martian intracrater splotches: Occurrence, morphology, and colors. *Icarus* **57,** 205–227.

THOMAS, P., AND C. WEITZ 1989. Sand dune materials and polar layered deposits on Mars. *Icarus* **81,** 185–215.

WENRICH, M. L., AND P. R. CHRISTENSEN 1994. Detectability of carbonate in unconsolidated and indurated sediments. *Lunar Planet. Sci.* **25,** 1485–1486. [Abstract]

WENTWORTH, C. K. 1922. A scale of grade and class terms for clastic sediments. *J. Geology* **30,** 377–392.

WHITE, B. R. 1979. Soil transport by winds on Mars. *J. Geophys. Res.* **84,** 4643–4651.

ZIMBELMAN, J. R., AND H. H. KIEFFER 1979. Thermal mapping of the northern equatorial and temperate latitudes of Mars. *J. Geophys. Res.* **84,** 8239–8251.